ACS OMEGA

Open Access

http://pubs.acs.org/journal/acsodf

Article

New Excipient For Oral Drug Delivery: CNC Derived From Sugarcane Bagasse-Derived Microcrystalline Cellulose

Shweta Mishra*

Cite This: *ACS Omega* 2024, 9, 19353−19362

Read Online

ACCESS | Metrics & More | Article Recommendations

ABSTRACT: Nanocrystalline cellulose (CNC) has emerged as a subject of researcher's interest because of its diverse attributes encompassing biocompatibility, sustainability, a high aspect ratio, and an abundance of −OH groups suitable for modifications. Sugarcane bagasse microcrystalline cellulose (SCBMCC) was used as the raw material for the preparation of CNC due to its pure cellulose content, which is mildly compromised by the pectin, hemicellulose, lignin, and other lignocellulosic components. In the present work, CNC was extracted from SCBMCC and used as a disintegrant. The classic hydrolysis technique was used for the preparation of CNC. Hydrolytic conditions were optimized using the response surface methodology (RSM). The optimized batch of CNC was characterized using techniques such as field-emission scanning electron microscopy (FESEM), transmission electron microscopy (TEM), X-ray diffraction (XRD), and attenuated total reflectance Fourier transform infrared (ATR-FTIR) spectroscopy. Notably, CNC prepared under a hydrolysis time of 90 min exhibited the highest crystallinity of 69.9%. The average particle size and zeta potential were found to be 145 nm and −34.4 mV, respectively. Thermal analysis suggested that an intermediate hydrolysis time resulted in CNC with enhanced thermal stability, showcasing its potential for pharmaceutical applications. Diclofenac potassium was used as the model drug to evaluate the disintegrant properties of CNC as an excipient. Tablets were prepared using the direct compression method. SCBMCC and CNC were used as disintegrants and were compared with the commercial product. The disintegration times (DTs) attained for the tablets prepared using CNC and SCBMCC are 219 and 339.83 s, respectively. The dissolution study of CNC showed a dissolution efficacy (DE%) of 66 and a mean dissolution time (MDT) of 12. The research findings showed that tablets prepared using CNC as disintegrants exhibited the fastest disintegration compared to other formulations.

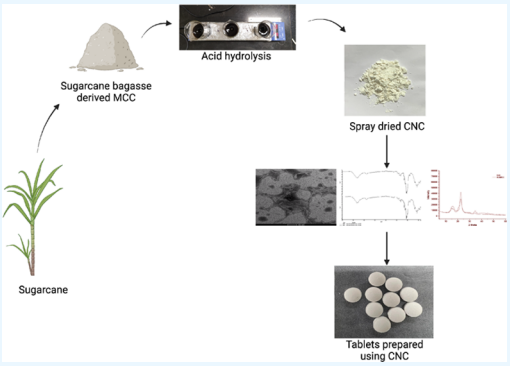

1. INTRODUCTION

Cellulose is one of the most inexhaustible natural polymers, which is widely present in the cell walls of all fibrous plants, algae, and oomycetes. Cellulose fibers can be isolated from wood (softwood and hardwood) and nonwood plants (agricultural waste), and it consists of 50−60% cellulose, 20−30% hemicellulose, and 10−25% lignin.[1] Cellulose, hemicellulose, and lignin are collectively known as lignocellulosic biomass. Cellulose is a homopolysaccharide consisting of β-D-glucopyranose units joined together by β-1,4-glycosidic linkages.[2] The degree of polymerization ranges from 10,000 to 150,000 depending on the source.[3] Hemicellulose is a branched polysaccharide that is structurally homologous to cellulose because it has a backbone composed of 1,4-linked β-D-hexosyl residues.[4] The units of lignin formation are guaiacyl(G), syringyl(S), and *p*-hydroxyphenyl. The three major pathways involved are as follows: the shikimate pathway, the phenylpropanoid pathway, and the synthesis of monolignols.[5] Cellulose is abundantly present in crop residue and fruit residue and is even obtained from different waste such as filter paper, newspaper, tetra pack, cigarette filter, and tea powder waste.[6]

India's diverse agro climate encourages the cultivation of numerous crops, including medicinal herbs, ornamental plants, decorative plants, vegetables, trees, root tubers, spices, and plantation crops. India is the second largest producer of fruits and vegetables in the world.[7] Lignocellulosic biomass is produced on a large scale yearly during harvesting, cultivation processing, and consumption of agricultural products. Sugarcane is the richest source of sucrose and plays a major role in sugar production globally. India is one of the leading countries in the production of sugarcane. Various states in India produce sugar as the first major crop for commercial purposes. India currently ranks second in cultivation area (5.11 million ha) and sugarcane production (303.83 million tons) next to Brazil. The

Received: January 15, 2024
Revised: April 5, 2024
Accepted: April 8, 2024
Published: April 18, 2024

number of sugar mills operating in India expanded from 29 to 520 within a year (1930−31), increasing the country's annual sugar output from 0.12 million to 34.97 million tons in 2022−24.[8] Large production of sugarcane has led to a high level of waste generation. In the past two decades, researchers have taken a keen interest in the utilization of waste in the nanoform for drug delivery, tissue engineering, and as a polymer matrix for nanocomposite films.[9,10]

The focus on renewable energy sources is obvious due to the concerns related to the use of fossil fuels and the ensuing greenhouse effect.[11] In this regard, agricultural waste is a promising source.[12,13] In addition, various waste products of agricultural origin have been used as raw materials for extracting industrially useful products, such as sugarcane bagasse microcrystalline cellulose (SCBMCC), nanocrystalline cellulose (CNC), and others. Sugarcane (*Saccharum officinarum*; Family: Poaceae or Gramineae) is a tall perennial plant that grows erect up to 5 to 6 m in height. It has four parts: root system, stalk, leaves, and inflorescence. It is cultivated in tropical and subtropical countries worldwide for the production of jaggery, sugar, and ethanol. Out of 195 countries, 24 are actively involved in sugarcane production. As of 2019, sugarcane production in India was 34,300 tons, accounting for 24.47% of the world's sugarcane production. Every year, these industries produce a large amount of byproducts such as sugarcane bagasse, dry leaves, sugarcane molasses, and sugarcane press mud. Bagasse is composed of 45−60% cellulose, 20−25% hemicellulose, 18−24% lignin, 1−4% ash, and less than 1% wax on a dry basis. Every year, a large amount of agricultural waste is collected around the globe.[14] For producing sugar from 10 wet tons of sugarcane, the industry collects 3 wet tons of sugar fiber waste, which ultimately causes environmental pollution if thrown in the open.[15,16] Given the scale, sugarcane bagasse is one of the most lucrative options for extracting cellulose without environmental concerns.

Various agricultural sources have been used for the extraction of microcrystalline cellulose (MCC) and CNC. Hasanin, Kassem, and Hassan prepared microcrystalline cellulose from olive stone using an acid hydrolysis technique. The prepared MCC was characterized using various techniques such as ATR-FTIR spectroscopy, TGA, XRD, and SEM. The prepared MCCs were compared with commercial MCC (Avicel 101), and the results showed good agreement in most properties between olive stone MCC and commercial MCC.[17] Kian, Jawaid, Ariffin, and Alothman used roselle fiber for the preparation of MCC by acid hydrolysis technique and obtained a yield of 29.7%; they prepared polylactic acid nanocomposites and used them for pharmaceutical applications. The MCC was purified, and partially depolymerized cellulose was prepared from bleached Kraft wood fiber, resulting in the existence of an amorphous part also in the structure, which gave flexibility to it and made it different from other types of CNC. The particle size of the MCC ranged from 10−50 μm to hundreds to thousands of microns in length. Preparing CNC from MCC has gained considerable attention because of its pure cellulose content, which is less compromised by hemicellulose, lignin, and waxes.[18] Prathapan, Thapa, Garnier, and Tabor prepared the CNC aqueous suspension from MCC and worked on zeta potential modulation based on different pH conditions with different concentrations of inorganic, organic salts, and surfactants to understand the correlation between the zeta potential and the roughness of CNC. Results depicted that ions and electrolytes offer an important way to control stability and film properties.[19] Cao, Huang, Li, Xu, Wu, Li, Lou, and Zong prepared biocompatible magnetic CNC (MCNC) by a simple coprecipitation cross-linking technique for the immobilization of lipase enzyme from Pseudomonas cepacia lipase (PcL). Results showed that PCL@MCNC was capable of effective catalysis, with a high yield of 43.4% and an enantiomeric excess of 83.5% of the product.[20]

Nanocellulose is a nanomaterial extracted from natural cellulosic materials. Cellulose nanocrystals are rigid rod-shaped crystals having a diameter of 5−10 nm and a length of 50−300 nm.[21] Unique properties of nanocrystalline cellulose such as biocompatibility, biodegradability, a high Young's modulus, high tensile strength, large surface area, and greater availability make nanocellulose significantly more different from other polymers. Size reduction is always a favored way to increase the surface area of a particle. An increase in the surface-to-mass ratio can enhance their performance.[22,23]

Because of the absence of a standardized nomenclature, the nanocellulose literature employs various terms to explain cellulose particle sets. The cellulose-based particles are classified into three different categories, which often vary from one another depending on the cellulose source materials and the extraction technique. Nanocellulose collectively represents multiple particle forms, including NFC, CNC, and BC, having a minimum of one dimension at the nanoscale.[24]

1.1. Nanofibrillated Cellulose (NFC). NFC particles are finer cellulose fibrils produced when specific techniques to facilitate fibrillation are incorporated into mechanical refining. NFCs are composed of 36 cellulose chains organized in an I_β crystal structure, having a high aspect ratio, are composed of ∼100% cellulose, and contain both amorphous and crystalline regions.[25]

1.2. Nanocrystalline Cellulose (CNC). Cellulose nanocrystals are rodlike particles that are prepared by acid hydrolysis of wood fiber, plant fiber, MCC, and NFC. They are made entirely of cellulose, have a high aspect ratio, are highly crystalline, and include a significant amount of I_β crystal structure. Because of their tapered ends, cellulose nanocrystals resemble whiskers. This is probably due to the acid hydrolysis process.[26]

1.3. Bacterial Nanocellulose (BC). Different bacteria secrete BC particles, which are microfibrils that have been cut from the bacterial cells. The resultant microfibrils have a significant aspect ratio, are several microns in length, and exhibit a shape that depends on the bacterium and growth conditions.[27]

The two primary methods of isolation used for extraction are acid hydrolysis and mechanical treatment. Pretreatment of plant and wood is usually performed for the partial removal of hemicellulose and lignin. Both the methods are explained in detail subsequently.

1.4. Acid Hydrolysis. Wood fiber, plant fiber, MCC, tunicate, algae, and bacteria are some of the cellulose sources from which crystalline particles are extracted using acid hydrolysis. In general, the "purified" starting material is incorporated into deionized water with a certain acid content. Most commonly, sulfuric acid is used because it gives particles a negative surface charge, which makes suspensions more stable. The mixture is diluted with deionized water and allowed to react for a certain period before the reaction is quenched. This mixture then undergoes a series of separation, filtration, and rinsing steps, followed by dialysis against deionized water to remove the remaining acid or neutralized salt. To eliminate any bigger agglomerates in the final cellulose nanoparticle suspension, a final centrifuge separation or filtering step might be utilized.[28]

https://doi.org/10.1021/acsomega.4c00497
ACS Omega 2024, 9, 19353−19362

1.5. Mechanical Treatment. The isolation of cellulose fibrils from MCC, tunicate, algae, and bacterial source materials has been accomplished mechanically by means of high-pressure homogenization, grinding, cryocrushing, high-intensity ultrasonic treatment, and microfluidization. In general, these activities result in strong shear, which induces transverse cleavage along the longitudinal axis of the cellulose microfibrillar structure, resulting in the extraction of long cellulose fibrils known as microfibrillated cellulose (MFC). Chemical treatments may be used after these mechanical operations to remove the amorphous material or chemically functionalize the particle surface.[29]

After the preparation of nanocellulose, it is characterized through various techniques. For identifying the functional groups, the FTIR technique is used; to analyze the crystallinity or amorphous nature, the XRD technique is used; the TGA technique is used to determine the thermal stability of nanocellulose. A Zeta sizer is used for determining the size and potential of nanocellulose. For morphological evaluation, various resolution techniques are used such as FESEM, TEM, and AFM.

Inspired by the literature studies, the present investigation attempted to prepare CNC by an acid hydrolysis technique at different time intervals and temperatures. The design of experiment (DoE) method was used for the optimization of CNC preparation parameters. The surface morphology was investigated by field-emission scanning electron microscopy (FESEM) and transmission electron microscopy (TEM); the crystallinity was calculated by XRD; and the thermal properties were determined by thermogravimetric analysis (TGA). Moreover, the CNC extracted in this study is used as a disintegrant for the oral delivery of diclofenac potassium as a model drug.

2. MATERIALS AND METHODS

2.1. Materials. SCBMCC prepared from sugarcane bagasse was received as a gift sample from Godavari Refineries Ltd. India. Sulfuric acid (95−98% purity) and dialysis tubes (cellulose membrane with an average flat width of 37.22 mm having a molecular weight cut off between 12,000 and 14,000) were purchased from the research lab and HiMedia Laboratory Pvt Ltd. India. Air jet-milling was performed to obtain a uniform size range of particles. A high-thrust jet of compressed air was used to reduce the particle size of SCBMCC. After jet-milling, the average particle size was around 10−60 μm. Diclofenac potassium was a gift sample received from Astamed Healthcare, Maharashtra. Cataflam 50 was used as a commercial reference for the study.

2.2. Preparation of CNC. SCBMCC was used as a starting material for the isolation of CNC. Briefly, 10 g of SCBMCC was hydrolyzed in 100 mL of (50 wt %) sulfuric acid solution at 45, 55, and 65 °C with different reaction times of 45, 90, and 135 min under magnetic stirring at speeds of 500, 1000, and 1500 rpm. After a specific reaction time, 10-fold chilled water was added to the suspension to quench the hydrolysis reaction, and the suspension was kept in the refrigerator overnight. The supernatant was decanted, and the pH of the solution was adjusted to 3 by repeated water washing, followed by centrifugation (Eppendorf, Germany) at 6000*g*. In the next step, the suspension dialyzed for 5−6 days in distilled water to achieve a pH of ∼5. To break down the unfractionated cellulose into nanometric particles and to form a homogeneously dispersed suspension, the sample was subjected to ultrasonication (Sigma Aldrich, VCX 500) for 30 min at 20 kHz. Thereafter, the suspension was left for 15 min to let the undesired large cellulose components settle down. Finally, the CNC suspension was collected and subjected to spray drying (LABULTIMA LU 222 Advanced).

2.3. Process Optimization of CNC Preparation Using the Design of Experiments Method. Based on the preliminary DoE experimental trials, it was concluded that the three main parameters that affected CNC preparation were the hydrolysis temperature, hydrolysis time, and stirring speed. The final screening was designed using the DoE (version 13) for factor screening. A Box−Behnken design (BBD) was used to generate higher-order response surfaces using fewer required runs than a normal factorial technique. BBD was employed to reduce the complexity as this requires only a few significant points from three-level factorial arrangements.[7] Hence, the total number of experiments needed was 17, and the z-average was used as the response in this study. The box is the boundary limit controlled at only 3 level figures as in −1, 0, and +1 to the experimental domain that represents the minimum, optimum, and maximum values. The boundary limits for the three input variables were 45−65 °C, 45−135 min, and 500−1500 rpm for hydrolysis temperature, hydrolysis time, and stirring speed, respectively, as shown in Table 1. The resulting response surface model was validated statistically using analysis of variance (ANOVA).

Table 1. Design of Experiment Inputs

parameter coding	actual parameters	low level (−1)	medium level (0)	high level (+1)
A	hydrolysis temperature (in °C)	45	55	65
B	hydrolysis time (in min)	45	90	135
C	stirring speed (in rpm)	500	1000	1500

2.4. Characterization of SCBMCC and CNC. *2.4.1. CNC Yield Calculation.* The percentage yield of CNC was calculated using eq 1

$$\text{yield } (\%) = M_2/M_1 \times 100\% \quad (1)$$

where M_1 is the initial total weight of SCBMCC, and M_2 is the dried weight of CNC samples

2.4.2. ATR-FTIR Spectroscopy. The FTIR spectra of the SCBMCC and CNC samples were recorded using an ATR-FTIR spectrometer (Make & Model: PerkinElmer 1600) for determining the functional groups in the range of 500−4000 cm^{-1} with a resolution of 4 cm^{-1}.

2.4.3. Morphological Features and Particle Size Analysis. Various techniques such as differential light scattering (DLS), field-emission scanning electron microscopy (FESEM), transmission electron microscopy (TEM), and atomic force microscopy (AFM) were used to study the particle size and morphological features of the extracted CNC.

2.4.3.1. Particle Size and ζ Potential Analysis. The particle size and ζ potential were measured by a Malvern Zeta sizer (Malvern, ZS 90). The CNC was diluted 100 times with DI water and sonicated for 15 min before measurement. All of the measurements were performed in triplicate.[30]

2.4.3.2. Field-Emission Scanning Electron Microscopy Analysis. FESEM analysis was performed to observe the morphological changes in CNC samples using a field-emission scanning electron microscope (Make & Model: JEOL JSM-7000F) operated at an accelerated voltage of 10−20 kV. Before

https://doi.org/10.1021/acsomega.4c00497
ACS Omega 2024, 9, 19353−19362

Table 2. A Response: Particle Size (*Y*1)

std. dev.	13.04		R^2	0.9289	
mean	207.26		adjusted R^2	0.8973	
C.V.%	6.29		predicted R^2	0.7973	
			adeq precision	15.3553	
B ANOVA					
source	sum of squares	Df	mean square	*F*-value	*P*-value	
model	19995.11	4	4998.78	29.39	<0.0001	significant
A-temp	1142.42	1	1142.42	6.72	0.0291	
B-time	1525.73	1	1525.73	8.97	0.0151	
BC	777.80	1	777.80	4.57	0.0612	
B^2	1803.01	1	1803.01	10.60	0.0099	
residual	1530.92	9	170.10			
lack-of-fit	1352.25	7	193.18	2.16	0.3523	not significant
pure error	178.67	2	89.33			
cor total	21526.03	13				

the FESEM analysis was carried out, aluminum stubs were used to mount the samples with carbon tapes and sprayed with a platinum coating to avoid overcharging. The sample surface was coated with gold under vacuum before analysis. Energy-dispersive X-ray diffraction (EDX) was performed to estimate the chemical composition of the CNC.[31]

2.4.3.3. Transmission Electron Microscopy Analysis. The morphology of the cellulose nanocrystals was examined using a transmission electron microscope (Make & Model: FEI Tecnai G2, F30). For TEM observation, a drop of 10 μL diluted cellulose nanocrystal suspension was deposited on a copper grid, the excess liquid was removed by blotting with filter paper after a minute, and it was allowed to dry for 15 min. 1 wt % phosphotungstic acid in water was used for the negative staining of the sample. Various particles (n = 25) were observed for the determination of the average length and diameter of the cellulose nanocrystals.[32]

2.4.3.4. Atomic Force Microscopy. AFM measurements of the cellulose nanocrystals were performed using a Bruker atomic force microscope (Make & Model: Veeco, Innova). Cellulose nanocrystals (1000 ppm aqueous concentration) were used for drop-casting. Samples were drop cast on a Mica sheet and air-dried to eliminate moisture. A Nano Scope (Veeco) analysis tool was used to assess the particle shape and topology in AFM images.

2.4.4. X-ray Diffraction Analysis. The degrees of crystallinity of SCBMCC and the spray-dried CNC samples were calculated using an X-ray diffractometer (Make & Model: XRD-6000, Shimadzu). A voltage of 30 kV, a current of 30 mA, a scanning range of 5°−60°, and a scanning speed of 2 °C/min were the parameters used for the analysis.

The crystallinity index was calculated using eq 2

$$\text{crystallinity index, CrI (\%)} = (I_{200} - I_{am})/I_{200} \quad (2)$$

where I_{200} is the crystallite peak corresponding to the intensity at approximately 22−23°, and I_{am} is the amorphous peak corresponding to the intensity at approximately 18−19.0°

2.4.5. Thermal Analysis. Thermogravimetric analysis (TGA) is defined as a thermoanalytical technique that is a dynamic combination of gravimetric analysis and oven drying. It reflects physical and chemical reactions including absorption, desorption, decomposition, oxidation, reduction, etc. About 5 mg of spray-dried CNC and SCBMCC were weighed using a TGA analyzer (Make & Model: PerkinElmer, TGA 8000). Thermogravimetric and derivative thermogravimetric analysis were performed in the temperature range of 30−900 °C at 20 °C min^{-1} heating rate under nitrogen gas flowing conditions.[33]

3. TABLET PREPARATION

SCBMCC and CNC were used as the disintegrating agents. Immediate-release (IR) tablets were prepared by direct compression method. The active ingredients and other excipients were weighed. Diclofenac potassium (50 mg) was mixed with 41 mg of lactose, 15 mg of disintegrant (SCBMCC or CNC), 2 mg of magnesium stearate, and 2 mg of talc, then passed through a 40# sieve, and blended for 5 min. The fixed weight (100 mg) of tablets was directly compressed using 6.35 mm flat punches. The compression force was set at 4N for minimizing the effect of physical parameters on drug dissolution.[34,35]

4. TABLET CHARACTERIZATION

4.1. Disintegration Test. A disintegration test apparatus (Make & Model: Erweka ZT 320) was used for determining the DT of the tablets. The test was carried out on six tablets using distilled water as a disintegration media at 37 ± 0.5 °C. The time taken for complete disintegration of the tablet, with no residue left on the screen, was measured in seconds. All measurements were performed in triplicate and the average mean was calculated.

4.2. In Vitro Dissolution Study. The tablet dissolution study was performed using a USP paddle apparatus II (Make & Model: Erweka DT 1410) in 900 mL of simulated gastric fluid. The apparatus was maintained at 37 ± 0.5 °C, with a rotation speed of 50 rpm, and the test was performed on 6 tablets. The sampling durations were 5, 10, 15, 30, and 60 min for the tablets. The amount of drug released was measured by UV−vis spectrophotometry (Make & Model: PerkinElmer, Lambda 25) at 279 nm wavelength. The tablets made with SCBMCC and CNC were compared with the marketed diclofenac potassium tablets. All measurements were performed in triplicate.

5. RESULTS AND DISCUSSION

5.1. Optimization of CNC Batches Using DoE. The model *F*-value of 29.39 shows that the model is significant and each variable has an effect on the response (Table 2B). The lack-of-fit (*P*-value 0.3523) was nonsignificant, indicating the significance of the model. The predicted R^2 of 0.8973 and the adj R^2 of 0.7973 are in reasonable agreement, and the difference is less than 0.2. The signal-to-noise ratio is 15.35, which indicates

https://doi.org/10.1021/acsomega.4c00497
ACS Omega 2024, 9, 19353−19362

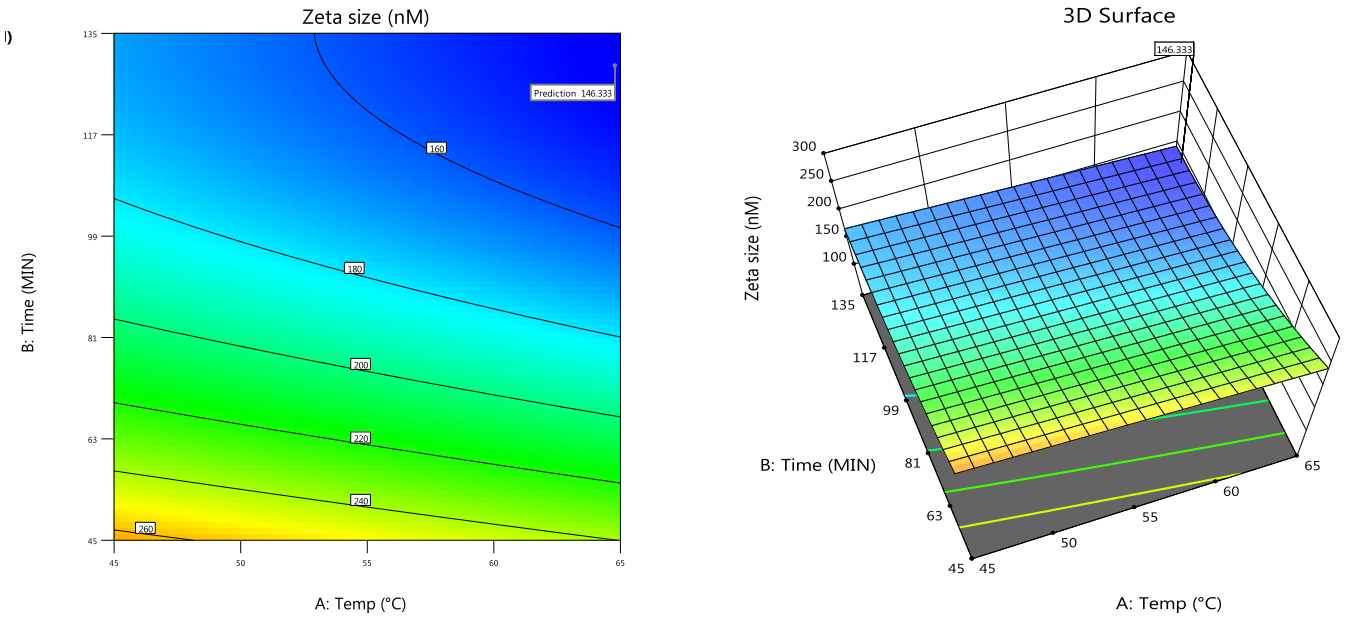

Figure 1. Contour plot and 3D surface response plot.

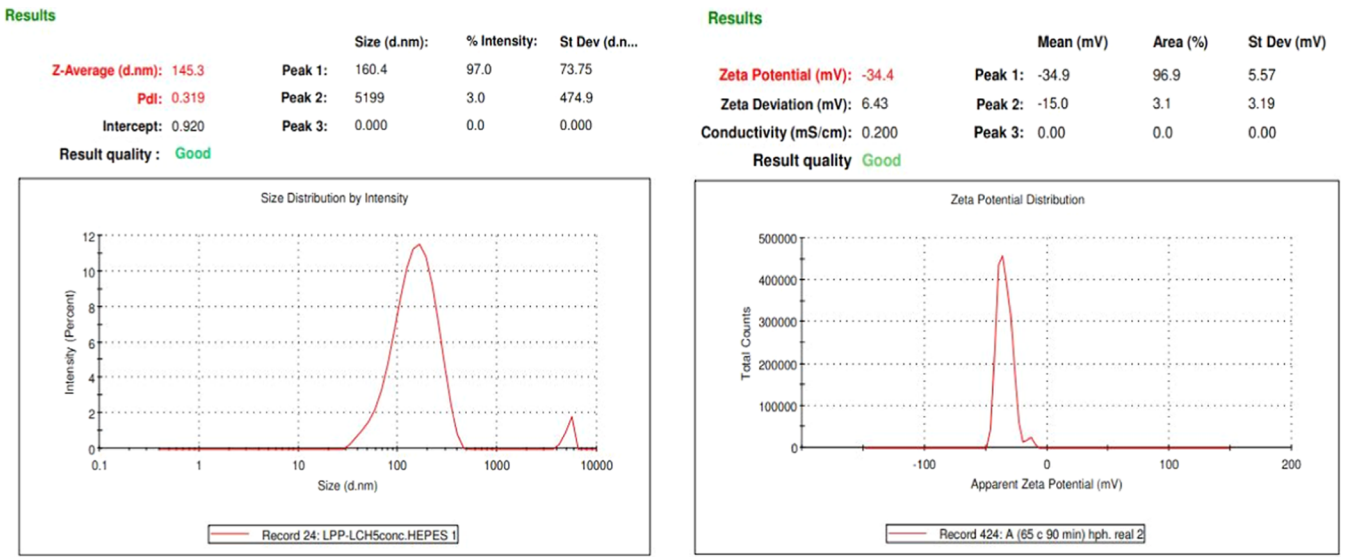

Figure 2. Particle size and ζ potential of CNC.

adequate signal. This model can also be used to navigate the design space.

Values of $P < 0.005$ indicate that the model terms are significant. The final regression equation for $Y1$ (particle size) is represented as eq 3

$$Y1 = +444.45357 - 1.19500A - 2.91825B - 0.000169AB + 0.011206B^2 \quad (3)$$

In this case, A, B, AB, and B^2 are significant model terms with a P-value (<0.0001), and A^2 is an insignificant model term. To reduce the insignificant term and to increase the model efficiency, backward elimination was performed. ANOVA for particle size was assessed after eliminating the insignificant model terms, and the result is depicted in Table 2B.

According to the fit summary, a modified model with a model P-value <0.0001 and a lack-of-fit P-value of 0.3523 were proposed for the particle size. As a result, the modified model for particle size was chosen as the best-fit model based on the fit summary. The final model adequacy was confirmed by a lack-of-fit test. As the P-value is >0.005, the null hypothesis for a lack of conformity could not be rejected. By using the 3D response surface, 2D contour plots were used to represent the relationship between independent and dependent variable responses (Figure 1). The figure shows the combined effect of temperature and reaction time on the particle size. The desired output of the model was indicated by a blue color. It was seen that the desired particle size can be achieved by keeping the reaction time at more than 90 min and the temperature higher than 55 °C.

5.2. CNC % Yield Calculation. The isolated CNC % yield is 29.9% with the optimized hydrolytic conditions (55% sulfuric acid concentration with a stirring speed of 1000 rpm at a reaction time of 90 min). Compared to the literature, Chen, Pang, Shen, Tong, and Jia isolated CNC from cotton pulp fiber, which provided 14% yield with 40% w/w sulfuric acid and 25% yield with 50% w/w sulfuric acid solution within 90 min.[36] Singla,

https://doi.org/10.1021/acsomega.4c00497
ACS Omega 2024, 9, 19353−19362

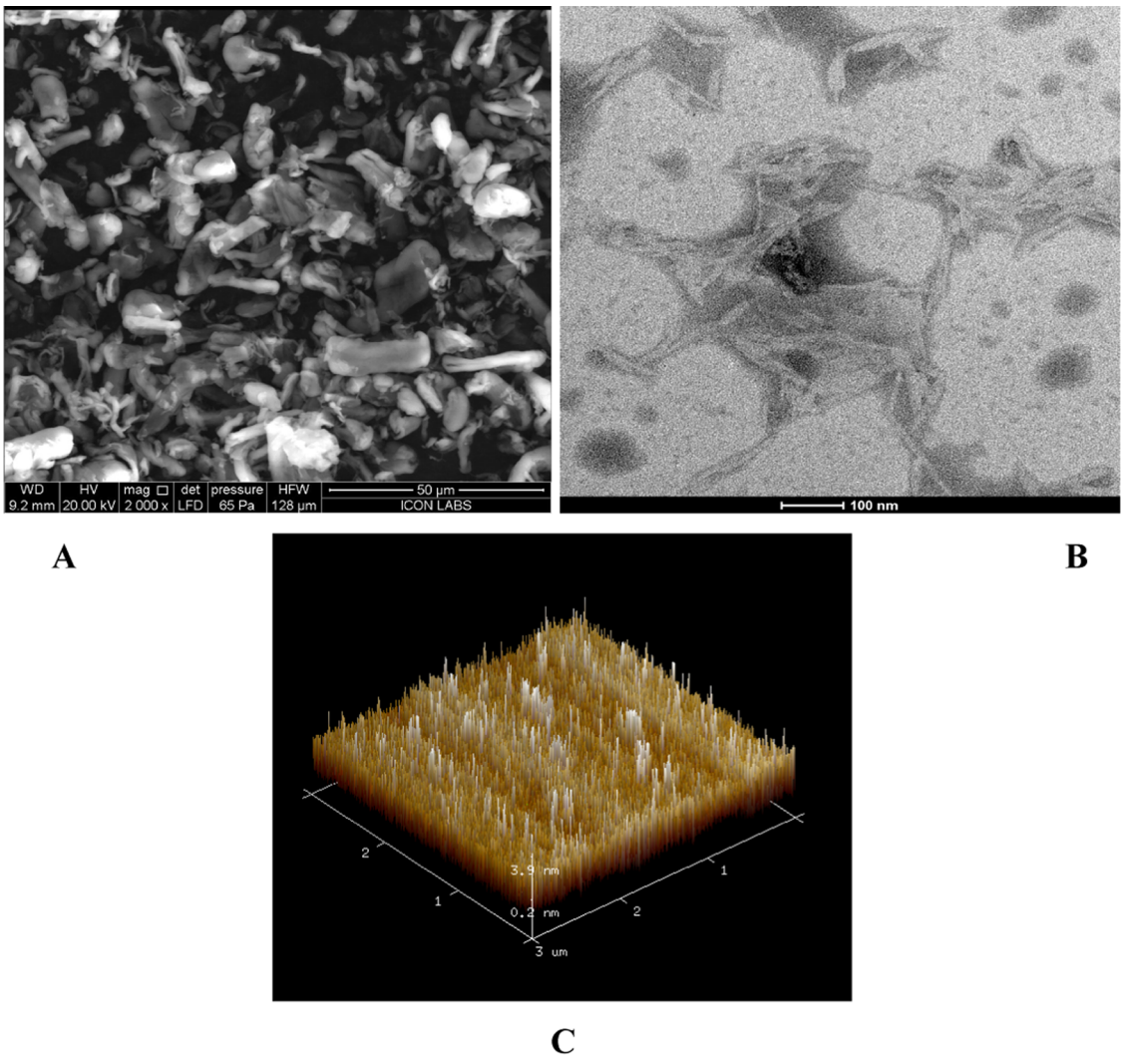

Figure 3. (A) SEM, (B) TEM, and (C) AFM images of CNC.

Soni, Kulurkar, Kumari, Mahesh S, Patial, Padwad, and Yadav prepared CNC from bamboo fibers, and results showed that the yield was around 22% with a reaction time of 45 min with a sulfuric acid concentration of 64%.[37]

5.3. Morphology and Particle Size Analysis. *5.3.1. Particle Size and ζ Potential.* The stability of the CNC suspension and particle size were assessed with the help of a Zeta sizer. Generally, a suspension that exhibits a ζ potential value lower than −30 mV or higher than 30 mV is considered to be stable. The particle size of the cellulose nanocrystals was found to be 145 nm, and the ζ potential was −34.4 (Figure 2), which shows the stability of the dispersion. The negative sign results from the negative charge of the sulfate group. This could have induced the strong electrostatic repulsion between CNC and water molecules, resulting in the overall stability of the CNC nanosuspension.

5.3.2. Morphological Evaluation. FESEM images of CNC prepared from SCBMCC are shown in Figure 3. Results showed a smooth and long fibrous structure. The image also exhibits a rough and peeling surface, which could be a result of the hydrolysis process.

TEM images revealed that the cellulose nanocrystals exhibit a rodlike structure. This might be due to the tiny nano-fragments that tend to agglomerate with elementary CNC crystallites by interfacial hydrogen bonds. Such an agglomeration was possibly proven by the TEM study displaying wider and larger widths in the size range of cellulose nanocrystals. This also showed that the cellulose nanocrystals were well aligned with each other in a large bundle, which is probably due to the short reaction time resulting in partial depolymerization of MCC microfibrils. Similar kinds of TEM images were observed for other cellulose nanocrystals prepared from date palm fiber,[38] wheat bran,[39] and pineapple leaf fibers.[40]

The AFM 3D image (Figure 3C) shows bright and dark sides, which represent crystalline and amorphous regions, respectively. Cellulose nanocrystals exhibit more of the bright side and less of the dark side, which could possibly be due to acid hydrolysis resulting in the cleavage of the amorphous region, which results in a decrease in the particle size. The highly dense crystallite area in the AFM topography image aligned with the TEM images.

Elemental analysis was performed using an energy-dispersive X-ray diffractometer (EDX diffractometer) attached to FESEM. As shown in Figure 4, the spectrum showed carbon and oxygen peaks corresponding to their binding energies, respectively. The major components found in CNC are carbon (C K, 41.67%) and oxygen (O K, 58.33%). Two small peaks are shown in the spectra, which are due to sulfate group impurities.

https://doi.org/10.1021/acsomega.4c00497
ACS Omega 2024, 9, 19353−19362

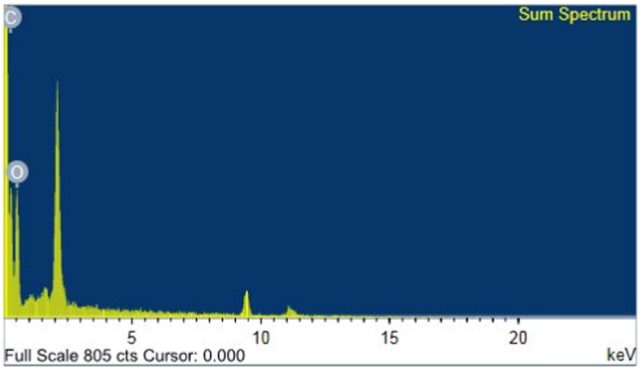

Figure 4. Elemental analysis of CNC.

5.4. ATR-FTIR Analysis. ATR-FTIR spectra of SCBMCC and CNC are shown in Figure 5. Almost similar spectra were observed for SCBMCC and CNC, with reduced sharpness showing no change in the functional groups. A broad absorption peak between 3343 cm^{-1} related to the (O−H) stretching bonds was observed in both spectra. Also, an absorption peak was observed at 2904 cm^{-1} corresponding to the (C−H) symmetric groups of cellulose.[41,42] Furthermore, another peak was observed at 1642 cm^{-1} due to water absorption.[43] Another peak appearing at 1379 cm^{-1} represented the (C−H) bonds of cellulose. Another protruding peak observed at 1060 and 1019 cm^{-1} was related to the (C−O−C) pyranose ring vibration of cellulose. At 897 cm^{-1}, characteristic peaks appear for CNC, due to the C−O−S bonding vibration in $C-O-SO^{3-}$ groups of cellulose sulfation, which is evidence of the hydrolysis process (Figure 6).

5.5. Thermal Properties. Thermal degradation properties of the SCBMCC and CNC were measured by thermogravimetric analysis. Both of the samples showed a single-peak degradation, which confirms that neither SCBMCC nor CNC has hemicellulose and lignin in it. In TGA, both samples showed gradual thermal transitions in the temperature range of 250−350 °C due to cellulose fibrils. For SCBMCC, the degradation at 330 °C is due to cellulose chain degradation. SCBMCC showed higher thermal degradation at 330 °C, whereas it occurred at 275 °C for CNC, which is probably due to the difference in the outer surface structures of SCBMCC and CNC, resulting from the process used for their preparation. The degradation weight temperature with the weight loss % is mentioned in Table 3.

5.6. XRD Analysis. The XRD pattern for cellulose I displays distinct diffraction peaks at 2θ values of approximately 14.5, 16.5, and 22.5, which were attributed to the planes of (110), (110), and (200), respectively. These assignments align with the characteristic diffraction peaks typical of cellulose I, affirming the crystalline structure of the analyzed cellulose sample. The XRD patterns of SCBMCC and CNC are shown in Figure 7. The crystallinity index was calculated using the Segal method and found to be 69.9%, with its highly intense peak at 22.8°, whereas SCBMCC showed 59.4% crystallinity. Sukyai, Anongjanya, Bunyahwuthakul, Kongsin, Harnkarnsujarit, Sukatta, Sothornvit, and Chollakup prepared CNC from MCC, which was derived from sugar date palm. They claimed an increase in the crystallinity by around 68%.[44] This supported the fact that the reduction of amorphous regions that are more degradable by hydronium ions tended to generate CNC crystallites with high crystallinity. This confirmed that SCBMCC was a reliable cellulose source for obtaining CNCs with higher crystallinity.

5.7. Tablet Characterization. *5.7.1. Disintegration Time.* Disintegrants play a very important role in the fast delivery of API. Figure 8 illustrates the difference in the disintegration times of tablets prepared using different disintegrants (commercial product, SCBMCC, and CNC). Tablets prepared using CNC showed the fastest disintegration, which was around half of the disintegration time of commercial tablets and tablets prepared using SCBMCC. Chengyu wang, Huijin huang, Min jia,

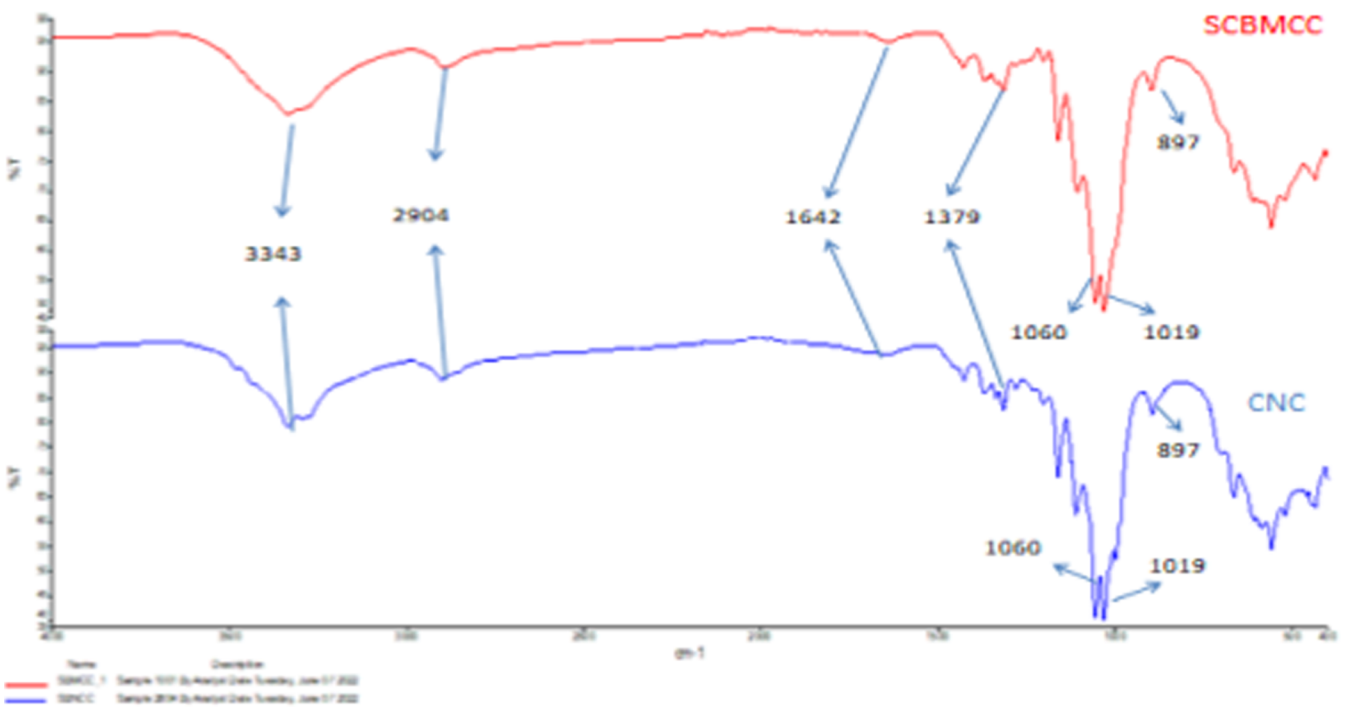

Figure 5. ATR-FTIR spectra of SCBMCC and CNC.

https://doi.org/10.1021/acsomega.4c00497
ACS Omega 2024, 9, 19353−19362

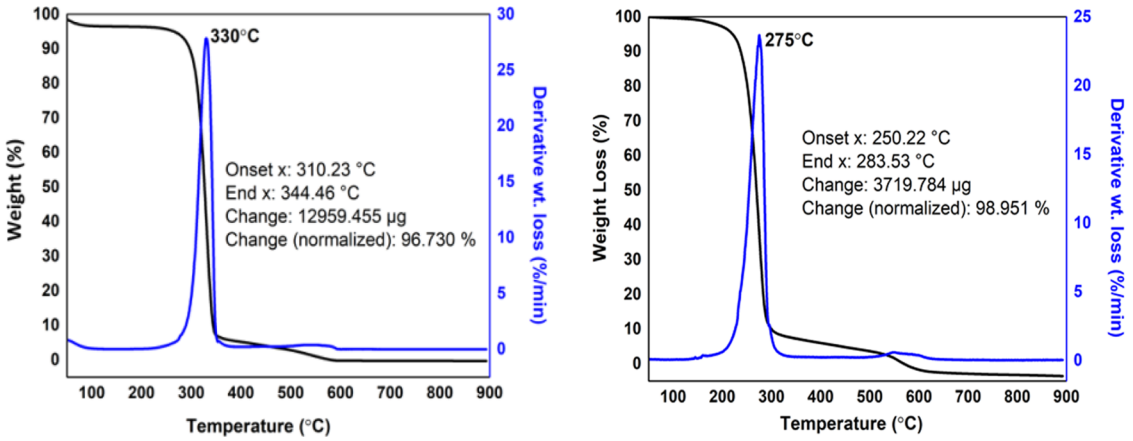

Figure 6. TGA curves of SCBMCC (left) and CNC (right).

Table 3. Degradation Weight Temperature with the Weight Loss %

sr. no.	degradation temperature (°C)	SCBMCC weight loss (in %)	CNC weight loss (in %)
1	50	98.561	100.005
2	100	96.599	99.627
3	150	96.45	99.112
4	200	96.335	97.179
5	250	95.667	80.856
6	300	88.687	9.955
7	350	7.135	7.274
8	400	5.222	6.001
9	450	4.054	4.799
10	500	2.817	3.638

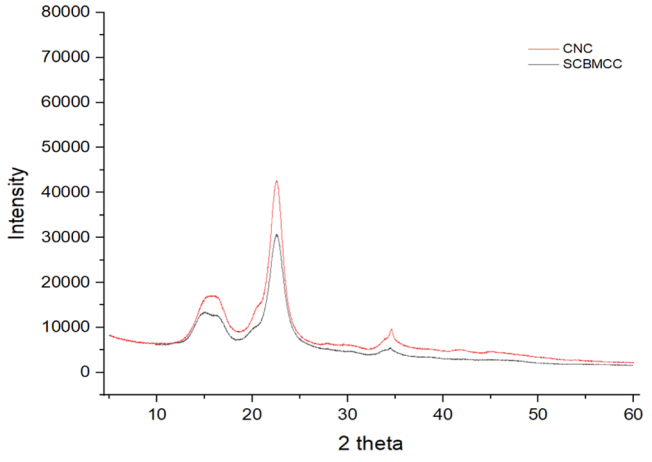

Figure 7. X-ray diffraction scattering of SCBMCC and CNC.

Shanshan jin, Wenjing zhao and Ruitao cha prepared calcium carbonate tablets using CNC, low-substituted hydroxypropyl cellulose (L-HPC), and MCC. All of the tablets were compared for their superdisintegration properties. Results showed that the disintegration time was higher when CNC was used in moderate proportions; an increasing CNC amount leads to a decrease in the disintegration time. NCC exhibited novel fluidity and hydrophilicity, which is a promising property in the disintegration process.[45] Emara, El-Ashmawy, Taha, El-Shaffei, Mahdey, and El-kholly used as a novel tablet excipient for improving the solubility and dissolution of meloxicam (BCS class II). Results

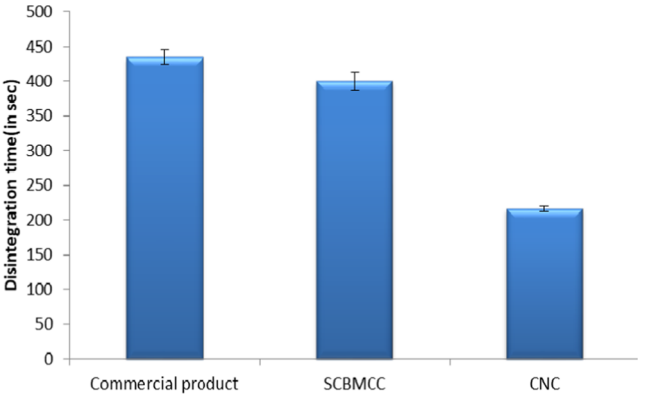

Figure 8. Disintegration times of SCBMCC, CNC, and the commercial product.

exhibited that CNC could be a promising tablet alternative to MCC.[46]

5.7.2. Dissolution Study. The % cumulative drug release (CDR) of the drug was found to be the highest in tablets prepared using CNC compared to tablets prepared using SCBMCC and the commercial product. The dissolution analysis is shown in Figure 9. The dissolution efficiency and the mean dissolution time were calculated, and CNC tablets showed a DE % of 66 and an MDT of 12, exhibiting good dissolution parameters when compared to the commercial reference, which

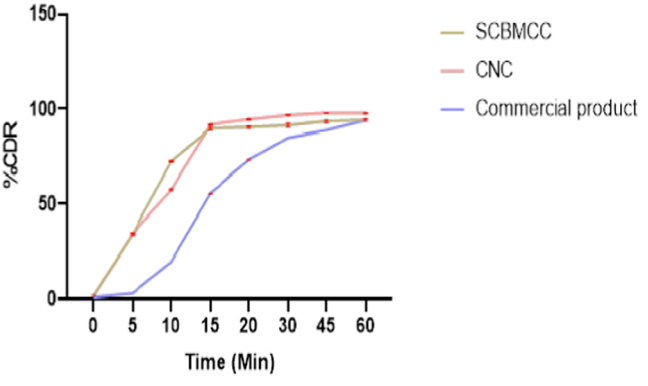

Figure 9. % Cumulative drug release of SCBMCC, CNC, and the commercial product.

https://doi.org/10.1021/acsomega.4c00497
ACS Omega 2024, 9, 19353−19362

showed a DE% of 58 and an MDT of 18.2, whereas SCBMCC tablets showed a DE% of 50 and an MDT of 11.6.

6. CONCLUSIONS

The isolation of CNC from SCBMCC following acid hydrolysis was successfully attempted. Optimized reaction conditions, including a sulfuric acid concentration of 55 wt %, a hydrolysis time of 90 min, and a reaction temperature of 55 °C at 1000 rpm, produced a maximum CNC yield of 29.9%. Notably, the hydrolysis reaction time played an important role in CNC preparation and significantly affected the yield. Less reaction time was detrimental to the total removal of the amorphous part, and an extremely longer time decreased the yield of CNC. The FESEM study showed elongated and intertwined fibers with a tapered end; also, the TEM images showed needle-like particles, thus confirming the expected nanocrystalline morphology. The properties exhibited by the extracted CNC qualified it as a potential material for use as a versatile carrier. The isolated CNC is used as a disintegrating agent for diclofenac potassium immediate-release tablets. All tablets made with CNC and SCBMCC were compared with the commercial tablets based on their DE% and MDT. Results showed that CNC tablets have a higher DE% and lower MDT compared to the other tablets because CNC has a greater surface area. These findings collectively affirm the potential of CNC as an emerging excipient for delivery, offering promising avenues for further exploration and refinement to identify additional desirable properties and applications.

AUTHOR INFORMATION

Corresponding Author

Shweta Mishra − *Shobhaben Pratapbhai Patel School of Pharmacy & Technology Management, SVKM's NMIMS, Mumbai 400056, India;* orcid.org/0000-0002-6480-0272; Email: mishrashweta264@gmail.com

Complete contact information is available at: https://pubs.acs.org/10.1021/acsomega.4c00497

Funding

The present research work did not receive any funds.

Notes

The author declares no competing financial interest.

ACKNOWLEDGMENTS

The author thanks SAIF, IIT Bombay, for sample analysis.

REFERENCES

(1) Lin, N.; Dufresne, A. Nanocellulose in biomedicine: Current status and future prospect. *Eur. Polym. J.* **2014**, *59* (July), 302−325.

(2) Dias, O. A. T.; Konar, S.; Leão, A. L.; Yang, W.; Tjong, J.; Sain, M. Current State of Applications of Nanocellulose in Flexible Energy and Electronic Devices. *Front. Chem.* **2020**, *8*, No. 420, DOI: 10.3389/fchem.2020.00420.

(3) Siqueira, G.; Bras, J.; Dufresne, A. Cellulosic Bionanocomposites: A Review of Preparation, Properties and Applications. *Polymers* **2010**, *2* (4), 728−765, DOI: 10.3390/polym2040728.

(4) Hasanin, M. S. Cellulose-Based Biomaterials: Chemistry and Biomedical Applications. *Starch - Stärke* **2022**, *74* (7−8), No. 2200060.

(5) Ilyas, R. A.; Sapuan, S. M.; Ishak, M. R. Isolation and characterization of nanocrystalline cellulose from sugar palm fibres (*Arenga pinnata*). *Carbohydr. Polym.* **2018**, *181*, 1038−1051.

(6) The potential of mango peel utilization for cellulose extraction by hydrothermal pretreatment Naiyasit Yingkamhaeng, Prakit Sukya

(7) Mishra, S.; Yadav, K. S.; Prabhakar, B. Application of quality by design approach to examine the effect of nanocrystalline cellulose extracted from agricultural waste as a disintegrant. *Chem. Pap.* **2023**, *77* (11), 7197−7213.

(8) Thiangtham, S.; Runt, J.; Saito, N.; Manuspiya, H. Fabrication of biocomposite membrane with microcrystalline cellulose (MCC) extracted from sugarcane bagasse by phase inversion method. *Cellulose* **2020**, *27* (3), 1367−1384.

(9) Ibrahim, N. A.; Hasanin, M. S.; Kamel, S. A new approach for improving the antimicrobial activity of cellulose pulp. *Inorg. Chem. Commun.* **2023**, *155*, No. 111009.

(10) Abou-Yousef, H.; Dacrory, S.; Hasanin, M.; Saber, E.; Kamel, S. Biocompatible hydrogel based on aldehyde-functionalized cellulose and chitosan for potential control drug release. *Sustainable Chem. Pharm.* **2021**, *21*, No. 100419.

(11) Mishra, S.; Kharkar, P. S.; Pethe, A. M. Biomass and waste materials as potential sources of nanocrystalline cellulose: Comparative review of preparation methods (2016 − Till date). *Carbohydr. Polym.* **2019**, *207* (October2018), 418−427.

(12) Kian, L. K.; Jawaid, M.; Ariffin, H.; Karim, Z. Isolation and characterization of nanocrystalline cellulose from roselle-derived microcrystalline cellulose. *Int. J. Biol. Macromol.* **2018**, *114*, 54−63.

(13) Pathak, P. D.; Mandavgane, S. A.; Kulkarni, B. D. Fruit peel waste: Characterization and its potential uses. *Curr. Sci.* **2017**, *113* (3), 444−454.

(14) El Achaby, M.; El Miri, N.; Hannache, H.; Gmouh, S.; Ben youcef, H.; Aboulkas, A. Production of cellulose nanocrystals from vine shoots and their use for the development of nanocomposite materials. *Int. J. Biol. Macromol.* **2018**, *117*, 592−600.

(15) Saravanan, N.; Sampath, P. S.; Sukantha, T. A. Extraction and Characterization of New Cellulose Fiber from the Agrowaste of *Lagenaria siceraria* (Bottle Guard) Plant. *J. Adv. Chem.* **2016**, *12* (9), 4382−4388.

(16) Anh, T. P. T.; Nguyen, T. V.; Hoang, P. T.; et al. Dragon Fruit Foliage: An Agricultural Cellulosic Source to Extract Cellulose Nanomaterials. *Molecules* **2021**, *26* (24), No. 7701, DOI: 10.3390/molecules26247701.

(17) Hasanin, M. S.; Kassem, N.; Hassan, M. L. Preparation and characterization of microcrystalline cellulose from olive stones. *Biomass Convers. Biorefin.* **2023**, *13* (6), 5015−5022.

(18) Kian, L. K.; Jawaid, M.; Ariffin, H.; Alothman, O. Y. Isolation and characterization of microcrystalline cellulose from roselle fibers. *Int. J. Biol. Macromol.* **2017**, *103*, 931−940.

(19) Prathapan, R.; Thapa, R.; Garnier, G.; Tabor, R. F. Modulating the zeta potential of cellulose nanocrystals using salts and surfactants. *Colloids Surf., A* **2016**, *509*, 11−18.

(20) Cao, S.; Huang, Y.; Li, X.; et al. Preparation and Characterization of Immobilized Lipase from Pseudomonas Cepacia onto Magnetic Cellulose Nanocrystals. *Sci. Rep.* **2016**, *6*, No. 20420, DOI: 10.1038/srep20420.

(21) Lin, N.; Dufresne, A. Nanocellulose in biomedicine: Current status and future prospect. *Eur. Polym. J.* **2014**, *59*, 302−325.

(22) Khoo, W. S.; Chow, H.; Ismail, R. Z. Sugarcane bagasse fiber and its cellulose nanocrystals for polymer reinforcement and heavy metal adsorbent: a review. *Cellulose* **2018**, *25*, 4303−4330, DOI: 10.1007/s10570-018-1879-z.

(23) Yang, H.; Chen, D.; van de Ven, T. G. M. Preparation and characterization of sterically stabilized nanocrystalline cellulose obtained by periodate oxidation of cellulose fibers. *Cellulose* **2015**, *22* (3), 1743−1752.

(24) Trache, D.; Tarchoun, A. F.; Derradji, M.; et al. Nanocellulose: From Fundamentals to Advanced Applications. *Front. Chem.* **2020**, *8*, No. 392, DOI: 10.3389/fchem.2020.00392.

(25) Yang, W.; Zhang, Y.; Liu, T.; et al. Completely Green Approach for the Preparation of Strong and Highly Conductive Graphene Composite Film by Using Nanocellulose as Dispersing Agent and Mechanical Compression. *ACS Sustainable Chem. Eng.* **2017**, *5* (10), 9102−9113.

(26) Kargarzadeh, H.; Ioelovich, M.; Ahmad, I.; Thomas, S.; Dufresne, A.Methods for Extraction of Nanocellulose from Various Sources. In *Handbook of Nanocellulose and Cellulose Nanocomposites*; Wiley, 2017; pp 1−49 DOI: 10.1002/9783527689972.ch1.
(27) Li, J.; Cha, R.; Mou, K.; et al. Nanocellulose-Based Antibacterial Materials. *Adv. Healthcare Mater.* **2018**, *7* (20), No. 1800334.
(28) Azizi Samir, M. A. S.; Alloin, F.; Dufresne, A. Review of Recent Research Into Cellulose Whiskers, Their Properties and Their Application in Nanocomposite Field. *Biomacromolecules* **2005**, *6* (2), 612−626.
(29) Putro, J. N.; Kurniawan, A.; Ismadji, S.; Ju, Y.-H. Nanocellulose based biosorbents for wastewater treatment: Study of isotherm, kinetic, thermodynamic and reusability. *Environ. Nanotechnol., Monit. Manage.* **2017**, *8*, 134−149.
(30) Mishra, S.; Prabhakar, B.; Kharkar, P. S.; Pethe, A. M. Banana Peel Waste: An Emerging Cellulosic Material to Extract Nanocrystalline Cellulose. *ACS Omega* **2023**, *8*, 1140−1145, DOI: 10.1021/acsomega.2c06571.
(31) Beltramino, F.; Roncero, M. B.; Torres, A. L.; Vidal, T.; Valls, C. Optimization of sulfuric acid hydrolysis conditions for preparation of nanocrystalline cellulose from enzymatically pretreated fibers. *Cellulose* **2016**, *23* (3), 1777−1789.
(32) Kovacs, T.; Naish, V.; O'Connor, B.; et al. An ecotoxicological characterization of nanocrystalline cellulose (NCC). *Nanotoxicology* **2010**, *4* (3), 255−270.
(33) Haafiz, M. K. M.; Hassan, A.; Zakaria, Z.; Inuwa, I. M. Isolation and characterization of cellulose nanowhiskers from oil palm biomass microcrystalline cellulose. *Carbohydr. Polym.* **2014**, *103* (1), 119−125.
(34) Singh, S.; Dodiya, T. R.; Singh, S.; Dodiya, R.; Bothara, S. B. Bio-based Polymer Isolated from Seeds of *Buchanania lanzan* Spreng with Potential Use as Pharmaceutical Mucoadhesive Excipient. *Int. J. Pharm. Sci. Nanotechnol.* **2020**, *13* (4), 5028−5035.
(35) Hasanin, M.; Fouad Taha, N.; Abdou, A. R.; Emara, L. H. Green decoration of graphene oxide Nano sheets with gelatin and gum Arabic for targeted delivery of doxorubicin. *Biotechnol. Rep.* **2022**, *34*, No. e00722, DOI: 10.1016/j.btre.2022.e00722.
(36) Chen, X. Q.; Pang, G. X.; Shen, W. H.; Tong, X.; Jia, M. Y. Preparation and characterization of the ribbon-like cellulose nanocrystals by the cellulase enzymolysis of cotton pulp fibers. *Carbohydr. Polym.* **2019**, *207*, 713−719.
(37) Singla, R.; Soni, S.; Kulurkar, P. M.; Kumari, A.; S, M.; Patial, V.; Padwad, Y. S.; Yadav, S. K. In situ functionalized nanobiocomposites dressings of bamboo cellulose nanocrystals and silver nanoparticles for accelerated wound healing. *Carbohydr. Polym.* **2017**, *155*, 152−162, DOI: 10.1016/j.carbpol.2016.08.065.
(38) Hachaichi, A.; Kouini, B.; Kian, L. K.; et al. Nanocrystalline cellulose from microcrystalline cellulose of date palm fibers as a promising candidate for bio-nanocomposites: Isolation and characterization. *Materials* **2021**, *14* (18), No. 5313, DOI: 10.3390/ma14185313.
(39) Cui, S.; Zhang, S.; Ge, S.; Xiong, L.; Sun, Q. Green preparation and characterization of size-controlled nanocrystalline cellulose via ultrasonic-assisted enzymatic hydrolysis. *Ind. Crops Prod.* **2016**, *83*, 346−352.
(40) Cherian, B. M.; Leão, A. L.; de Souza, S. F.; Thomas, S.; Pothan, L. A.; Kottaisamy, M. Isolation of nanocellulose from pineapple leaf fibres by steam explosion. *Carbohydr. Polym.* **2010**, *81* (3), 720−725.
(41) Evans, S. K.; Wesley, O. N.; Nathan, O.; Moloto, M. J. Chemically purified cellulose and its nanocrystals from sugarcane baggase: isolation and characterization. *Heliyon* **2019**, *5* (10), No. e02635.
(42) Hemmati, F.; Jafari, S. M.; Kashaninejad, M.; Barani Motlagh, M. Synthesis and characterization of cellulose nanocrystals derived from walnut shell agricultural residues. *Int. J. Biol. Macromol.* **2018**, *120*, 1216−1224.
(43) Akhlaghi, S. P.; Zaman, M.; Mohammed, N.; et al. Synthesis of amine functionalized cellulose nanocrystals: Optimization and characterization. *Carbohydr. Res.* **2015**, *409*, 48−55.
(44) Sukyai, P.; Anongjanya, P.; Bunyahwuthakul, N.; et al. Effect of cellulose nanocrystals from sugarcane bagasse on whey protein isolate-based films. *Food Res. Int.* **2018**, *107*, 528−535.
(45) Wang, C.; Huang, H.; Jia, M.; Jin, S.; Zhao, W.; Cha, R. Formulation and evaluation of nanocrystalline cellulose as a potential disintegrant. *Carbohydr. Polym.* **2015**, *130*, 275−279.
(46) Emara, L. H.; El-Ashmawy, A. A.; Taha, N. F.; El-Shaffei, K. A.; Mahdey, E. S. M.; El-kholly, H. K. Nano-crystalline cellulose as a novel tablet excipient for improving solubility and dissolution of Meloxicam. *J. Appl. Pharm. Sci.* **2016**, *6* (2), 032−043.

https://doi.org/10.1021/acsomega.4c00497
ACS Omega 2024, 9, 19353−19362